Available online at www.sciencedirect.com

ScienceDirect

Advances in Space Research 61 (2018) 2198–2213

ADVANCES IN SPACE RESEARCH (a COSPAR publication)

www.elsevier.com/locate/asr

3D radar wavefield tomography of comet interiors

Paul Sava [a,*], Erik Asphaug [b]

[a] Center for Wave Phenomena, Colorado School of Mines, 1500 Illinois Street, Golden, CO 80401, USA
[b] Lunar and Planetary Laboratory, University of Arizona, 1629 E University Blvd, Tucson, AZ 85721, USA

Received 30 October 2017; received in revised form 25 January 2018; accepted 28 January 2018
Available online 2 March 2018

Abstract

Answering fundamental questions about the origin and evolution of small planetary bodies hinges on our ability to image their surface and interior structure in detail and at high resolution. The interior structure is not easily accessible without systematic imaging using, e.g., radar transmission and reflection data from multiple viewpoints, as in medical tomography. Radar tomography can be performed using methodology adapted from terrestrial exploration seismology. Our feasibility study primarily focuses on full wavefield methods that facilitate high quality imaging of small body interiors. We consider the case of a monostatic system (co-located transmitters and receivers) operated in various frequency bands between 5 and 15 MHz, from a spacecraft in slow polar orbit around a spinning comet nucleus. Using realistic numerical experiments, we demonstrate that wavefield techniques can generate high resolution tomograms of comets nuclei with arbitrary shape and complex interior properties.
© 2018 COSPAR. Published by Elsevier Ltd. All rights reserved.

Keywords: Comet; Radar; Wavefield; Imaging; Tomography

1. Introduction

This paper makes the case for a direct imaging approach to learning the detailed geology of cometary nuclei (e.g. Asphaug, 2010). We demonstrate the applicability of sounding radar data acquired from orbit about a comet nucleus, together with coherent data processing using wave based imaging, to reconstruct a detailed 3D image of its deep interior.

The ideal target of this investigation is a <20 km diameter Jupiter Family Comet (JFC) nucleus, for three reasons. First, comets are profoundly important objects scientifically, as discussed below. Second, the CONSERT experiment of the Rosetta mission (Kofman et al., 2015; Herique et al., 2016) discovered that cometary nuclei **are radar-transparent** to depths of kilometers, and are therefore especially well suited to global 3D imaging at frequencies between 5 and 15 MHz. Third, the JFCs have been scattered inwards fairly recently by the giant planets, many of them on Earth-approaching orbits inside Jupiter with periods of around 5–6 years; this makes them the most accessible targets for low-cost science exploration of the outer solar system.

1.1. The importance of comets

In contrast to the visible planets whose movements are like clockwork, comets blaze through the sky in seemingly random apparitions that have been recorded since the dawn of astronomy. Not only are comets spectacular and unusual, but they are vital to the scientific understanding of the Solar System (A'Hearn et al., 1995). Comet dynamics began with the prediction that 1P/Halley would reappear in 1758, an event that validated celestial mechanics. Since then, far more detailed studies of comet orbits, and their rotation states and water production rates (measured in the coma), have led to detailed models of the physics of

* Corresponding author.
E-mail address: psava@mines.edu (P. Sava).

https://doi.org/10.1016/j.asr.2018.01.040
0273-1177/© 2018 COSPAR. Published by Elsevier Ltd. All rights reserved.

gravitational and non-gravitational forces (Samarasinha and Belton, 1995). The thousands of discovered comets trace the migration of the giant planets (Levison and Duncan, 1997); their physical structures also bear record of their collision history, indicative of the state of dynamical excitement of the swarm.

Jupiter Family Comets are accessible and deeply important science targets, and have been visited by a number of highly successful missions: NASA's Deep Space 1 to 19P/Borrelly, Stardust to 81P/Wild and 9P/Tempel, and Deep Impact to 9P/Tempel and 103P/Hartley. ESA's Rosetta mission to 67P/Churyumov-Gerasimenko was the first spacecraft to orbit a comet nucleus (Glassmeier et al., 2007). Yet despite these and other related missions there are major unanswered questions concerning origins, dynamics, geology and cosmochemistry. Rosetta revolutionized comet science, but left several questions on the table related to one of its primary science objectives: *Explain the comet's origin – where it was formed, the relationship of its materials to those found in interstellar space, and whether or not it witnessed in the formation of our solar system.* A primary origin is favored by Rosetta scientists (Massironi et al., 2015), but this appears to be in conflict with the large degree of collisional evolution predicted by solar system dynamical models. For example, a combination of visible imaging and thermal and radiometry data suggests that the comet nucleus may consist of meter-scale "pebbles" through and through, as argued by Blum et al. (2017). This would be consistent with studies of radar pulse width by Ciarletti et al. (2017), but remains an important hypothesis. A primordial pebble structure would rule out collisions faster than ~1 m/s between the lobes of the nucleus according to Blum et al. (2017), but would allow for primordial < 1 m/s collisions of the sort modeled by Jutzi and Asphaug (2015). Right or wrong, it would not allow for post-formation collisional evolution which is a key aspect of contemporary ideas for planet formation.

At the crux of this uncertainty and conflict is the basic lack of knowledge of internal structure and global geology. Only with geologic knowledge can we begin to relate surface landforms, processes and cosmochemistry to present and past activity throughout the volume of a comet nucleus. This is necessary in order to assemble a picture of its long history, which according to many (Weissman, 1986; Weidenschilling, 1997; Belton et al., 2007; Sierks et al., 2015) contains a structural record from before there were planets. According to others the dynamical evolution of the solar system requires the catastrophically disruptive evolution of the small icy bodies population, much in the way that all of the Main Belt asteroids that are smaller than 100–200 km are thought to be fragments of larger parent bodies that have been evolved to a greater or lesser extent (Bottke et al., 2007). For example, according to Morbidelli and Rickman (2015), in the standard disk model an object of the size of 67P/C-G would have experienced repeated catastrophic collisions, in conflict with primordial or "pebble" accretion models.

For a cometary nucleus, born in the formation region of the giant planets, exiled to the region beyond Neptune, and transported back into the interior of the Solar system to be visible and accessible from Earth, either as an original body or perhaps a fragment of a disrupted Kuiper Belt Object (KBO), the global geology is the record of its formation, dynamics and geochemistry. However, our geological intuition is based on Earth observations, so we must be careful to recognize that the geologic forces on a several-kilometer-diameter primitive body are different, especially due to the lack of atmosphere or liquid water, and due to the presence of a weak gravity field, around 1/1000 that of Earth. Nevertheless, we can investigate such objects using some of the same exploration techniques, given how much we have learned about the geology of Earth from radar and seismic imaging (Clærbout, 1976; Berkhout, 1982; Clærbout, 1985). With appropriate modifications, the same geophysical technologies can be applied to cometary nuclei.

Although seismology on Earth can be optimized to produce high definition imaging of upper crustal structure, the deployment of seismic arrays on a small body without much gravity is a formidable endeavor, and even then the successful interpretation of the data is far from ensured due to their likely sparsity. The attempted deployment of the Philae lander to the surface of 67P/C-G, the first lander ever sent to the surface of a comet nucleus, illustrates the difficulty in merely coming to rest on the surface (Biele et al., 2015), let alone deploying an array of sensors.

Because of its remote sensing nature, and because electromagnetic waves penetrate deep into cold icy structures, radar imaging is extremely well suited to cometary nuclei, being a technique that does not require landers. For mission simplicity, we emphasize a monostatic approach, acquiring all our data from orbit (Safaeinili et al., 2002; Kofman and Safaeinili, 2004; Asphaug et al., 2010; Sava et al., 2015; Grimm et al., 2015; Kofman et al., 2015). We take advantage of the important science heritage from Rosetta's bistatic CONSERT experiment, that transmitted at 90 MHz between the orbiter and the lander Philae (Kofman et al., 2007). This experiment showed that 67P/C-G has a transparent (low permittivity) interior at MHz frequencies (Kofman et al., 2015; Bibring et al., 2015), consistent with a cold, porous interior. At MHz frequencies, radar can be used to study structure (via imaging of reflectors and maps of dielectric properties) at meter and decameter scale, to reveal layers and vents and impact craters and whatever else may extend deep into the interiors of cometary nuclei.

More directly related to our proposed imaging methodology are the MARSIS and SHARAD radar reflection instruments onboard ESA's Mars Express and NASA's Mars Reconnaissance Orbiter, respectively. These have produced high definition radargrams and derived products (Foss et al., 2017) that have revolutionized our understanding of the climate cycles of Mars (Phillips et al., 2011) and the origin of Polar Layered Deposits and buried glaciers

(Plaut et al., 2009). Mars PLDs are good analogues, in some respects to cometary nuclei: both are kilometers-thick cold ice-dominated masses exhibiting layered structures with visible and thermal expression at the surface. Both are excellent radar science targets because of their low electromagnetic losses at MHz frequencies, and the fundamental geologic record they reveal of global volatile evolution. However, cometary nuclei are different in one major respect: we cannot assume a flat surface with a "nadir" point from which we can model away surface "clutter". Radar echoes come back to the transmitter from everywhere on and inside the nucleus, making its imaging **an intrinsically 3D problem.**

Gravity is another means of accessing the deep interior of a planetary body. A low-order mass distribution can be reconstructed by analysis of Doppler-derived spacecraft velocities around the nucleus. While the GRAIL gravity images of the Moon are spectacularly detailed (Zuber et al., 2013), nothing of this sort can be obtained at an asteroid or comet, because the noise (from spacecraft operations, and from radiative forcing on the solar arrays and bus) is the same as around the Moon, whereas the signal is orders of magnitude weaker. Nevertheless we emphasize that a mission designed to acquire the best radar reflection data around a comet nucleus is also going to acquire the best possible gravity data by a single spacecraft: long duration in close orbit with minimal spacecraft operational noise. Thus, when considering radar reflection tomography, one should keep in mind that the mass distribution inside the nucleus can be resolved to around 1 km scales as a separate data product, obtained from Doppler velocities of the communications band.

Despite the many successes in comet science and missions to Jupiter Family Comets and related bodies, several hypotheses for internal structure are on the table, each with its implications for solar system formation and dynamical evolution, and for cosmochemistry.

In this paper we do not investigate in detail the imaging attributes of each one of these scenarios. Instead, we focus on development of imaging methodology, tomography in particular, that has the capability to image at appropriate resolution such that these structures can be differentiated from one-another. We consider models of real exterior shapes, and with complex interiors characterized by sharp contrasts of physical properties.

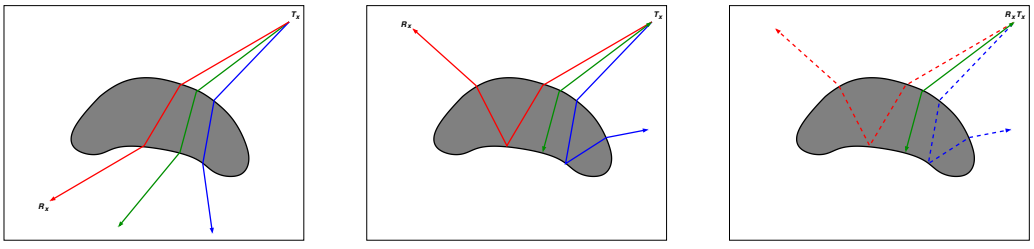
1.2. Imaging strategies

Wavefield techniques successfully image complex geologic targets, as demonstrated in exploration seismology (e.g. Clærbout, 1976; Berkhout, 1982; Clærbout, 1985) or global seismology (e.g. Dahlen and Tromp, 1998; Nolet, 2008). Such methods are superior to alternative simplified techniques primarily because they take into account the full waveforms of the observed reflections, and not only the associated propagation times. Similar methodology can be applied with minor modifications to radar imaging of small icy bodies, which is the approach we take in this paper.

Wavefield imaging experiments can be classified in two main categories:

- *Transmission experiments* (Fig. 1(a)): waves emanating from a transmitter antenna propagate inside a body and continue to a receiver antenna located on the opposite side of the body relative to the transmitter.
- *Reflection experiments* (Fig. 1(b)): waves emanating from a transmitter antenna propagate inside the body, reflect off surfaces of physical contrasts, and return to a receiver antenna. Often, the transmitter and receiver antennas are co-located, thus describing a monostatic reflection experiment (Fig. 1(c)).

Here, we advocate a hybrid technique that functions effectively as a transmission experiment, but uses monostatic radar reflection data. This configuration exploits the fact that the radar antenna is mounted on a single spacecraft that orbits the small body, thus providing illumination from all directions. It also takes advantage of the fact that the shape of the small body is known with high precision prior to conducting the radar experiment, for example using stereo photogrammetry (Preusker, 2015; Cremonese et al., 2015) or LIDAR (Smith et al., 2001, 2010). This configuration is not only effective in imaging inside complex comet nuclei, but it is also computationally efficient, thus facilitating high-end iterative techniques like



(a) (b) (c)

Fig. 1. Schematic representation of (a) transmission experiments, (b) bistatic reflection experiments, and (c) monostatic reflection experiments.

wavefield tomography (Tarantola, 1984; Gauthier et al., 1986; Pratt and Worthington, 1990; Woodward, 1992; Bunks et al., 1995; Pratt, 1999; Sirgue and Pratt, 2004; Operto et al., 2004; Sava and Biondi, 2004; Plessix, 2006; Virieux and Operto, 2009).

We emphasize that 3D data processing and imaging are not only possible, but in fact necessary, because they provide multi-directional illumination of the comet interior, akin to a 3D medical tomograph. Approaching the imaging problem this way eliminates the need to consider separately off-plane reflections, and therefore we do not need to consider imaging clutter, as all reflections illuminate the interior and can be used for tomography. Moreover, we show that wavefield datuming removes the long propagation time in free space, thus increasing computing efficiency of subsequent imaging. Such datuming also opens-up the possibility to compensate for track spacing and the antenna radiation pattern (we do not address these topics in this paper).

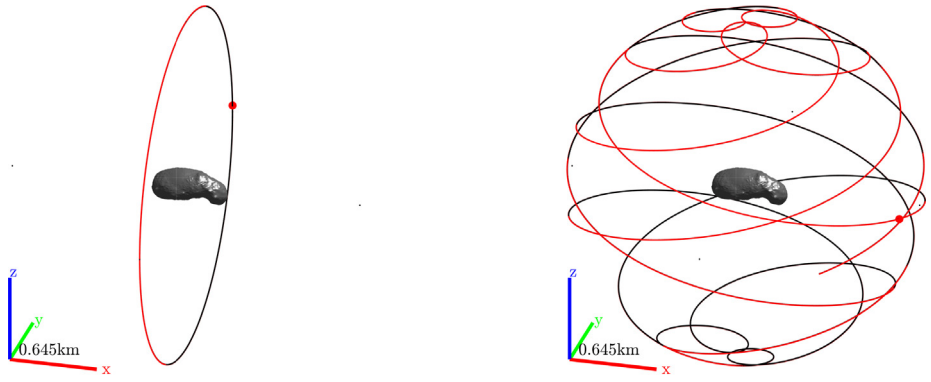
In the following sections we illustrate how orbital radar acquisition enables 3D data processing and then proceed to discuss about (1) the exploding reflector model which underlies our technique, (2) 3D datuming from orbit to the comet surface using analytic Green's functions, and (3) 3D multiscale radar wavefield tomography. We conclude with a simulation of a realistic 3D example using the small body shape of asteroid Itokawa and a complex icy interior structure.

2. Acquisition geometry

We consider the problem of imaging inside a comet nucleus using radar waves generated by a spacecraft in polar orbit, Fig. 2(a). The nucleus is assumed to be spinning around an axis that defines its polar direction. Moreover, the spacecraft is assumed to be moving slowly in a polar orbit, such that the orbital period is significantly higher ($> 5\times$) than the nucleus rotation period (Safaeinili et al., 2002). As a consequence, seen from a coordinate system attached to the comet nucleus, the spacecraft moves along a helical trajectory that allows it to observe the nucleus from multiple directions, Fig. 2(b). We assume a radar antenna pointing in the nadir direction, such that the nucleus is permanently in its direct line of sight. The example in Fig. 2 uses an imaging target with a rotation period of 12.1 hrs. The spacecraft orbit has a radius of 1.3 km and a period 52.9 hrs. Fig. 2 depicts the orbital tracks for 5 days of acquisition time.

The nucleus illumination with radar waves depends on the acquisition duration. If the rotation and orbital periods are carefully chosen to avoid tuning, then the orbits do not repeat, thus increasing the diversity of the illumination directions as a function of acquisition time. For example, Fig. 3 depicts the progressively increasing orbital density for the scenario shown in Fig. 2, and for acquisition durations of 15, 30, 60 and 90 days, respectively. The 90 day acquisition time achieves dense coverage from all directions and azimuths. We note that, although the spacecraft orbital speed is constant, the coverage is not uniform. The polar regions have much higher coverage density than equatorial regions, and are in fact significantly oversampled from an imaging point of view. Nevertheless, the 90 day acquisition is perfectly adequate to achieve dense equatorial coverage.

The main message of this analysis is that the comet nucleus imaging problem is intrinsically three-dimensional. Data are densely distributed along an acquisition sphere, and thus all reflections from the nucleus interior are captured, regardless of whether they originate from the nadir direction, or any other direction. We are processing all acquired data at once, and do not assign any special meaning to data that are sequentially acquired along the orbital tracks. Processing in the acquisition track coordinate system only leads to complications and approximations that degrade imaging accuracy. For example, seen from this perspective, there are no "off plane" reflections,



(a) (b)

Fig. 2. Spacecraft trajectory represented in a space reference frame. The orbiter is in a stable polar trajectory and the comet is spinning at a faster rate than the orbiter period. (b) Spacecraft trajectory represented in a comet reference frame. The orbiter appears to follow a helical trajectory relative to the fixed comet.

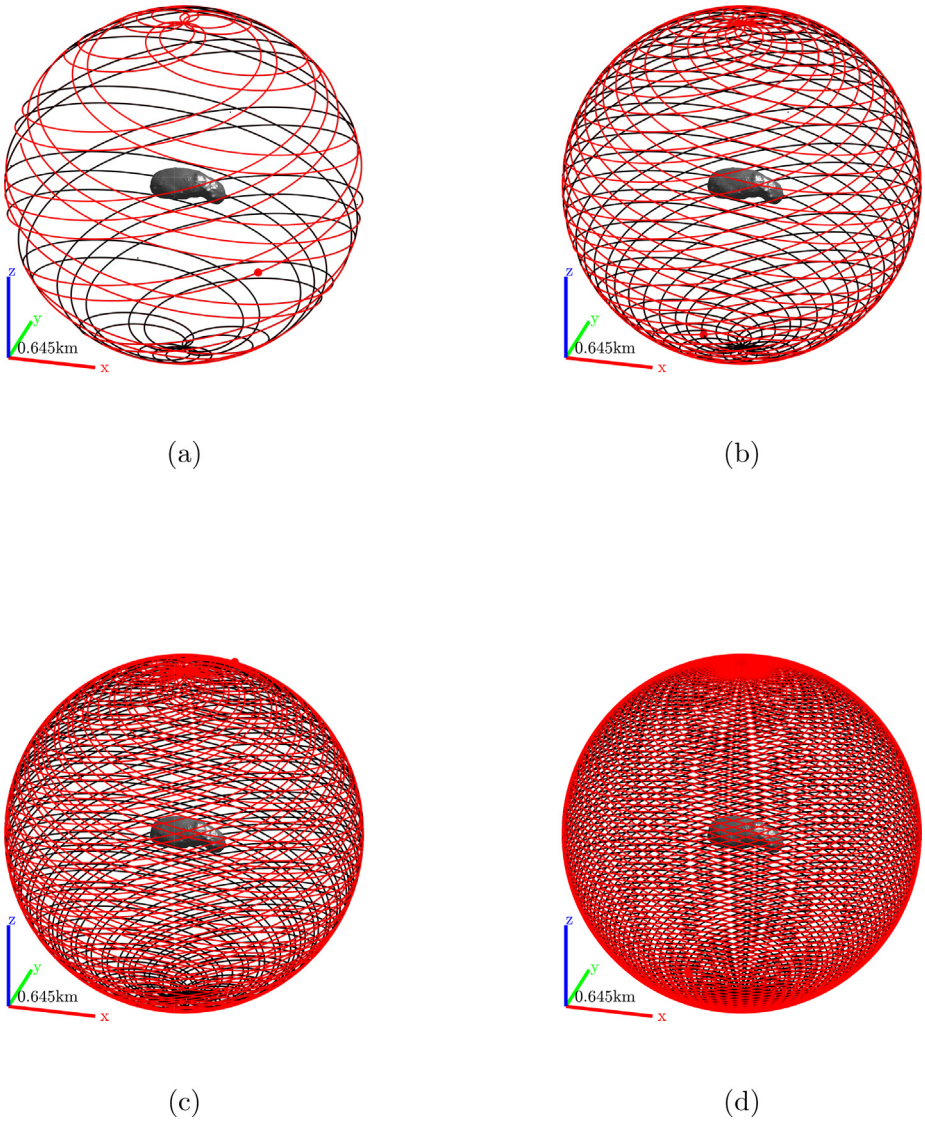


Fig. 3. 3D orbital coverage for different acquisition durations: (a) 15 days, (b) 30 days, (c) 60 days, and (d) 90 days. The sampling points progressively cover the entire orbital sphere.

and therefore there is no need to process data to eliminate components that do not follow a two-dimensional processing paradigm (in other words, there is no reflection "clutter", but just reflection data).

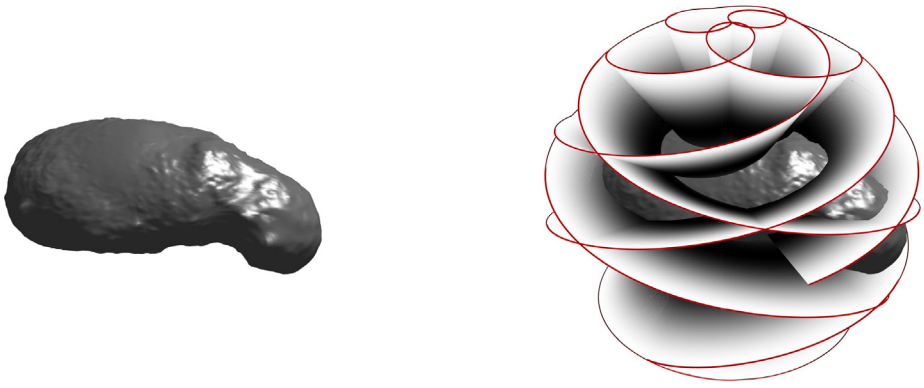
Fig. 4 illustrates this idea for the 3D object depicted in Fig. 4(a). If we were to process data acquired along the helical paths depicted in Fig. 2(b) using a 2D mindset, then we would have to fold the resulting section as seen in Fig. 4 (b). This is extremely complicated and may require additional postprocessing to register different portions of the helical slices. This approach would also require interpolation to generate (imperfect) 3D models. As we discuss next, this is not necessary at all if we proceed from the beginning with 3D data processing.

A potential drawback of 3D data processing is high computational cost. In the following sections, we discuss mechanisms to mitigate this problem by using the exploding reflector model and wavefield datuming to the comet surface.

3. Exploding reflector model

Wavefield imaging with monostatic radar experiments can be described based on the so-called "exploding reflector model" (Clærbout, 1985). This imaging strategy is highly effective in reducing the imaging computational cost, by treating all the data as components of a single experiment. Therefore, all acquired data are propagated at once inside the imaging body, in contrast with alternative strategies that propagate data from every observation point separately. This $1/N$ cost reduction, where N represents the number of monostatic experiments which could be in the order of 10^6, is essential in order to make iterative and thus computationally-intense imaging techniques feasible.

The key idea behing the exploding reflector model is that waves propagating from a transmitter **T** return to a receiver **R** colocated with the transmitter if they reflect at 90° on the reflecting interfaces. This is a consequence of Snell's



(a) (b)

Fig. 4. (a) Shape model and (b) representation of 2D slices corresponding to track based processing. Such 2D imaging is misleading since radar waves from an orbital antenna reflected inside the comet are not confined to the 2D helical planes. In addition, visualization of 2D helical slices is difficult and nonintuitive.

law which states that the angles of incidence and reflection must be equal; if the incidence is at 90°, then the return path to the receiver antenna is identical with the incidence path from the transmitter antenna. This concept covers the vast majority of the events captured by a monostatic experiment, although lower amplitude alternative propagation paths are possible (Clærbout, 1985).

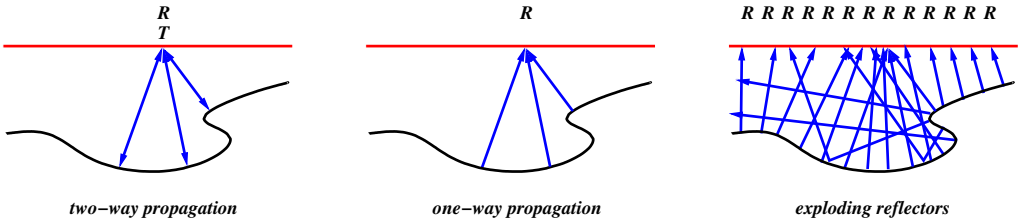
Under the 90° reflection assumption, the propagation paths from the transmitter to the reflector and from the reflector to the receiver are identical, since waves simply change direction 180° while interacting with any interface, Fig. 5(a) and (b). Thus, the two-way reflected data are equivalent with what we would observe if the sources were represented by all interfaces triggered at the same initial time, Fig. 5(c). In this case, the propagation time is exactly half as compared with the actual reflection time, which means that we can equivalently image the observed data with the exploding reflector model either with the actual velocity by scaling the reflection time in half, or with the actual reflection time by reducing the velocity in half.

The exploding reflector model is capable of describing propagation in complex media characterized by spatial velocity variation, as well as reflectors of arbitrary shapes and orientation. We are primarily using for wavefield tomography the reflections from the comet surface; we argue later that the more complex the surface shape, the higher the resolution of the inverted interior model.

4. Wavefield imaging

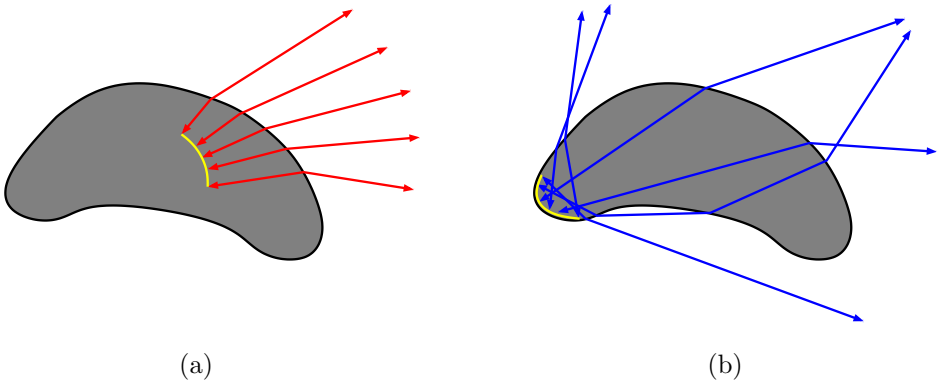
Wavefield imaging techniques have a long track record in the context of seismic exploration (Berkhout, 1982; Clærbout, 1985), and also in the context of global seismology (Dahlen and Tromp, 1998; Nolet, 2008). These techniques can be applied with relatively minor modifications to radar imaging, both in the context of Ground-Penetrating Radar (Reynolds, 2011; Jol, 2008; Miller et al., 2010), and also in the context of Synthetic Aperture Radar (Prati et al., 1990; Sava et al., 2015; Foss et al., 2017).

Two types of imaging techniques can be applied to data acquired with a single spacecraft in orbit around a comet nucleus, i.e. for monostatic experiments:



(a) (b) (c)

Fig. 5. Schematic description of the exploding reflector model. (a) A wave departing transmitter **T** returns to the receiver **R** (same as the transmitter **T**) if the reflection occurs at normal incidence. (b) Under certain assumptions, this path is equivalent with that of a wave departing the reflector at normal incidence and traveling directly to the receiver **R**. The data for the path **T**-reflector-**R** at true velocity are equivalent with the data for the path reflector-**R** at half velocity. (c) The data at all **T**/**R** pairs can be constructed simultaneously if all reflectors act as sources.



(a) (b)

Fig. 6. (a) Schematic representation of a reflection experiment. The imaging objective of migration is to correctly position reflectors (yellow line) inside the comet nucleus. (b) Schematic representation of a transmission experiment. The imaging objective of tomography is to infer the physical properties throughout the comet nucleus by enforcing the condition that the back-side reflectors are imaged on the known nucleus shape. (For interpretation of the references to colour in this figure legend, the reader is referred to the web version of this article.)

- *Wavefield migration*, Fig. 6(a): a process designed to position interfaces between different material properties in the comet interior using time reversal. This method requires knowledge of the propagation speed throughout the comet interior in order to place unknown reflectors at their correct position.
- *Wavefield tomography*, Fig. 6(b): a process designed to evaluate the radar wave propagation speed throughout the interior of the comet. Unlike migration which positions unknown reflectors in the subsurface using a known velocity, tomography requires information about a known reflector to evaluate the propagation speed at every point inside the comet.

The exploding reflector model strategy is applicable equally well to both imaging strategies. Both techniques can handle models with arbitrary velocity distribution and reflector geometry. Moreover, these imaging approaches are complementary to one-another: knowledge of propagation speed enables accurate positioning of reflectors; knowledge of reflectors facilitates constraints on the propagation velocity. Wavefield migration is fairly straightforward and capable of accurately imaging reflectors (Sava et al., 2015), if an accurate velocity model is available. Thus, we do not discuss migration in this paper, and focus instead on the more challenging and non-linear wavefield tomography problem wich generates the velocity needed for migration.

Accurate wavefield imaging relies on reconstruction of radar wavefields inside the object under investigation from data recorded outside the object. For example, we can characterize radar wave propagation using a scalar wave equation which accounts for the dielectric medium parameters, permeability $\mu(\mathbf{x})$ and permittivity $\epsilon(\mathbf{x})$, as well as attenuation controlled by the medium conductivity $\sigma(\mathbf{x})$:

$$\mathbf{L}u \equiv \mu\epsilon\frac{\partial^2 u}{\partial t^2} + \mu\sigma\frac{\partial u}{\partial t} - \nabla^2 u = f(\mathbf{x},t). \tag{1}$$

The source function $f(\mathbf{x},t)$ can exist at any location in space, $\mathbf{x}$, but it can also be localized, e.g., on the nucleus contour. Eq. (1) implies that the attenuation controlled by the medium conductivity is spatially variable, but does not change as a function of frequency. To first order, this is a reasonable assumption to model medium attenuation in typical icy geology. Moreover, for low-frequency radar waves, we can assume that attenuation is negligible (Bar-Cohen, 2016), and therefore we can use a simplified scalar wave equation (Aki and Richards, 2002)

$$\mathbf{L}u \equiv \mu\epsilon\frac{\partial^2 u}{\partial t^2} - \nabla^2 u = f(\mathbf{x},t). \tag{2}$$

which can also be written equivalently as

$$\mathbf{L}u \equiv \frac{1}{v^2}\frac{\partial^2 u}{\partial t^2} - \nabla^2 u = f(\mathbf{x},t) \tag{3}$$

to describe the propagation and scattering inside comet nuclei. The scalar wave equation formulation allows for faster computing relative to a more accurate vector wave equation, although it does not account for second-order effects, like wave attenuation or polarization changes during propagation. Nevertheless, the techniques described in the following can be applied equally well to more complex wave equations. Specifically, the quantity u from Eq. (1) could represent each component of the magnetic and electric fields, and thus the equation can characterize vector field propagation in a medium with negligible depolarization.

The applicability of wavefield tomography to imaging inside a comet nucleus depends on the penetration depth, because we will later assume that the radar pulse crosses the comet nucleus, reflects off the back-side and returns to the spacecraft. The penetration distance depends on the instrumentation, i.e. the radar antenna power and sensitivity, but also on the material properties. CONSERT penetrated ~2 km at 90 MHz; assuming that the penetration decays inverse proportionally with the frequency, the penetration at 5 MHz should be ~20 km and at 15 MHz should be ~6 km (Heggy et al., 2012). Therefore, we can conclude that comets with mean nuclei diameter in the

order of <20 km are perfect targets for the techniques advocated in this paper.

5. Wavefield datuming

As indicated earlier, we consider a spacecraft in slow orbit around a comet nucleus. We also assume that in order to insure orbital stability and safety, the spacecraft is relatively far from the nucleus (Scheeres et al., 1998), i.e. at least several mean radii away. Thus, the reflected data acquired at the spacecraft with a significant delay representing two-way propagation time in free space from the orbiter to the nucleus and back.

For illustration, consider the model depicted in Fig. 7 (a). The shape is inspired by asteroid Itokawa, while the interior is designed to simulate a mix of two icy materials with different physical properties, i.e. propagation speeds. Fig. 8 depicts the monostatic reflection data simulated for the acquisition geometry depicted in Fig. 3(d). The variable $T(days)$ represents acquisition time (slow-time) up to a 90 day mission, while variable $t(\mu s)$ represents one-way reflection time (fast-time), as required by the exploding reflector model. The strongest reflections correspond to the nucleus surface (i.e. transition from space to icy geology), Fig. 7(b); the earlier reflector is an expression of the near-side, while the later reflector represents the back-side. Other reflections correspond to interior interfaces, which are significantly weaker than the exterior reflections given their relatively lower contrast between regions characterized by different physical properties. We assume that radar operations are within tens of km of the comet nucleus, and thus they must take place when the presence of coma gas is minimal, so we ignore its electromagnetic contribution.

It is apparent from Fig. 8 that all reflections occur with significant delay due to the long propagation time (fast-time) in free space from orbit to the nucleus and back. Imaging directly from orbit would require unnecessary calculations to account for this delay. It is important for subsequent processing and wavefield tomography to significantly reduce the computational cost and avoid unnecessary computations corresponding to propagation outside the nucleus.

Our strategy to avoid such redundant calculations is to relocate data from orbit to the surface of the nucleus, Fig. 9. This datuming process is relatively quick and exact, since it is done in free space characterized by a constant velocity medium, and can be accomplished using analytic Green's functions (Aki and Richards, 2002), as discussed in detail next.

Let $d(\mathbf{s},t)$ represent the exploding reflector data at all positions $\mathbf{s}$ on the nucleus surface as a function of fast-time t. The corresponding data in orbit at positions $\mathbf{o}$ as a function of fast-time are $h(\mathbf{o},t)$. The radar wavefields d and h are related by

$$h(\mathbf{o},t) = \int_{\Omega} d\mathbf{s}\, d(\mathbf{s},t) * \mathcal{G}(\mathbf{o},\mathbf{s},t), \tag{4}$$

where the symbol $*$ indicates time convolution, and Ω represents the surface of the comet nucleus. The quantity $\mathcal{G}(\mathbf{o},\mathbf{s},t)$ are Green's functions defined by

$$\mathcal{G}(\mathbf{o},\mathbf{s},t) = \mathcal{A}(\mathbf{o},\mathbf{s},\mathbf{n})\delta\left(t - \frac{\|\mathbf{o}-\mathbf{s}\|}{c}\right), \tag{5}$$

where $\|\dots\|$ indicates the Euclidian distance between the points of coordinates $\mathbf{s}$ and $\mathbf{o}$, and c is the speed of light in free space. The quantity $\mathcal{A}$ is an amplitude factor that depends on the distance between points on the surface and in orbit, as well as the normal to the orbit surface $\mathbf{n}$. For example, the amplitude term can be defined as

$$\mathcal{A}(\mathbf{o},\mathbf{s},\mathbf{n}) = \frac{\mathcal{W}(\mathbf{o},\mathbf{s},\mathbf{n})}{4\pi\|\mathbf{o}-\mathbf{s}\|c^2}. \tag{6}$$

The weight function $\mathcal{W}$ captures the orientation between the vectors $\mathbf{o}-\mathbf{s}$ and $\mathbf{n}$, and thus can represent the radar antenna pattern useful to eliminate contributions from points on the nucleus surface that are not within the antenna line of sight. For example, we could define

$$\mathcal{W}(\mathbf{o},\mathbf{s},\mathbf{n}) = \mathbf{n}\cdot(\mathbf{o}-\mathbf{s}), \tag{7}$$

although many alternative definitions are possible.

A practical method to infer the data on the nucleus surface d from the data observed in orbit h is to solve an optimization problem. Defining all the orbital and surface data by vectors $\mathbf{h}$ and $\mathbf{d}$, respectively, we can define a linear datuming operator $\mathbf{G}$ based on Eq. (4) as

$$\mathbf{h} = \mathbf{G}\mathbf{d}. \tag{8}$$

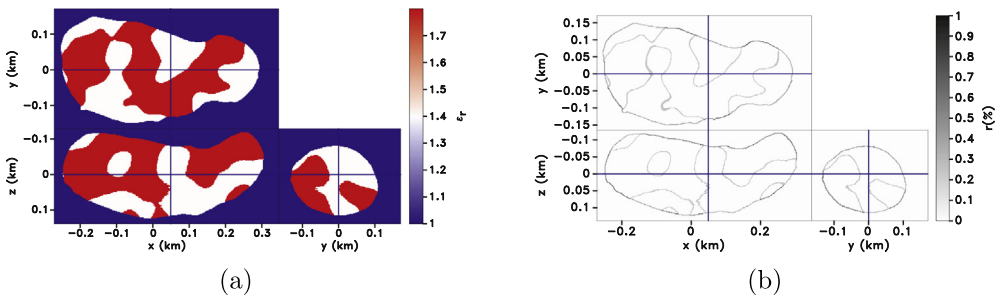


Fig. 7. (a) True 3D interior comet nucleus model used for a monostatic wavefield tomography experiment. (b) Normalized reflectivity map derived from the model in panel (a). The surface reflectors are the strongest, and dominate the reflected wavefields.

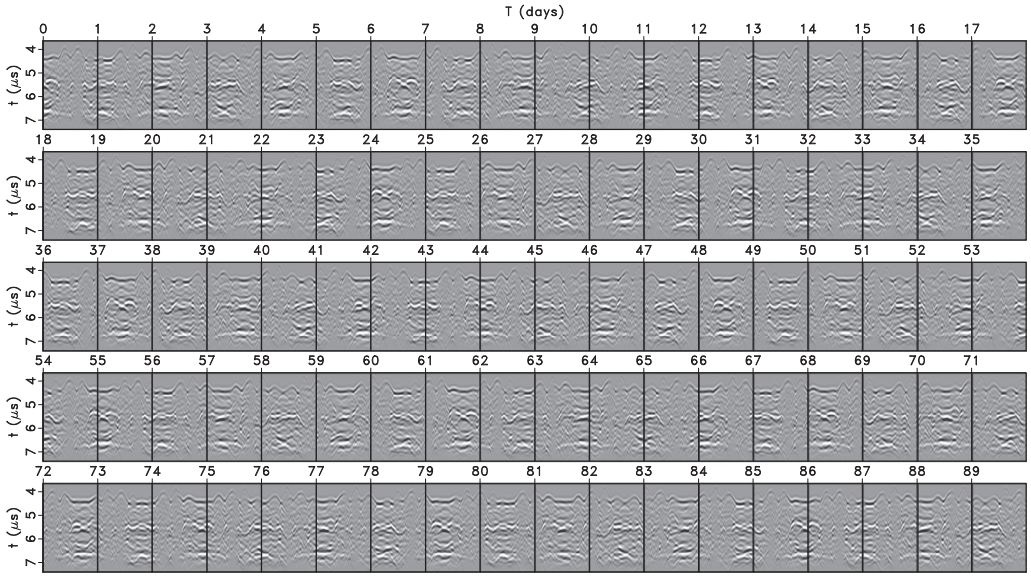


Fig. 8. Simulated radar reflection data for the orbiter trajectory depicted in Fig. 3(d). Variable $T(days)$ represents acquisition time, slow-time, and variable $t(\mu s)$ represents the one-way reflection time, fast-time. The strong event around 4 μs depicts the reflection for the nucleus exterior closest to the orbiter; the strong event around 6 μs represents the reflection from the back-side of the nucleus.

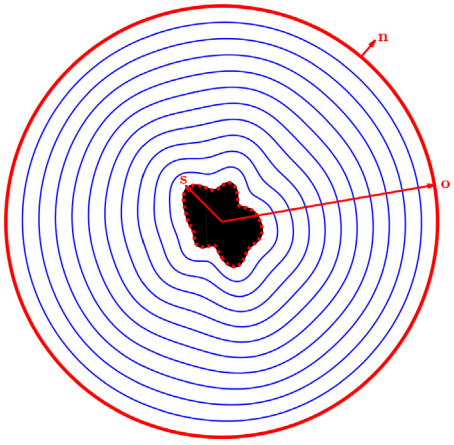


Fig. 9. Schematic representation of wavefield datuming. Radar reflections observed in orbit (solid red line) are remapped to the surface of the comet nucleus (dashed red line) using constant velocity wavefield datuming (blue lines). (For interpretation of the references to colour in this figure legend, the reader is referred to the web version of this article.)

With this definition, we can seek to find the surface data $\mathbf{d}$ by minimizing an objective function J defined as (Tarantola, 1987)

$$J(\mathbf{d}) = \frac{1}{2}\|\mathbf{h} - \mathbf{G}\mathbf{d}\|^2. \tag{9}$$

The optimum datumed wavefield has the known least-squares solution

$$\widehat{\mathbf{d}} = \left(\mathbf{G}^\top \mathbf{G}\right)^{-1}\mathbf{G}^\top \mathbf{h}. \tag{10}$$

The symbol $^\top$ indicates the adjoint operator. In practice, the linear operator $\mathbf{G}$ is large, so computing the inverse of $\mathbf{G}^\top\mathbf{G}$ is prohibitively expensive. Instead, we can compute the solution given by Eq. (10) using an iterative numeric method, e.g. conjugate gradient (Fletcher, 1987; Nocedal and Wright, 2000).

Fig. 10 shows the forward simulated exploding reflector wavefield (left panel) for the model depicted in Fig. 7(a), compared with the wavefield reconstructed on the nucleus surface using the linear datuming operator (right panels). Using the datumed data on the nucleus surface achieves massive computational speed-up, which is essential for iterative optimization methods like wavefield tomography, discussed in the following section.

We note that this datuming mechanism allows for purposeful data regularization, for example by using the objective function

$$J(\mathbf{d}) = \frac{1}{2}\|\mathbf{h} - \mathbf{G}\mathbf{d}\|^2 + \frac{1}{2}\|\mathbf{R}\mathbf{d}\|^2. \tag{11}$$

The symbol $\mathbf{R}$ represents a regularization operator that enforces smoothness of the zero-mean wavefield on the nucleus surface. We do not use this approach in this paper because it is not needed for the considered scenario with long acquisition time (slow-time), but merely highlight the possibility to handle data acquired over shorter time intervals and infill missing data. For the 90 day acquisition scenario, the essential features of the simulated and reconstructed wavefields depicted in Fig. 10 match very well, even without data regularization.

In the following, we use the data datumed to the nucleus surface, together with the exploding reflector model, to infer model parameters inside the comet nucleus using wavefield tomography.

6. Wavefield tomography

In developing the tomography problem, we rely on the data corresponding to the entire acquisition time datumed

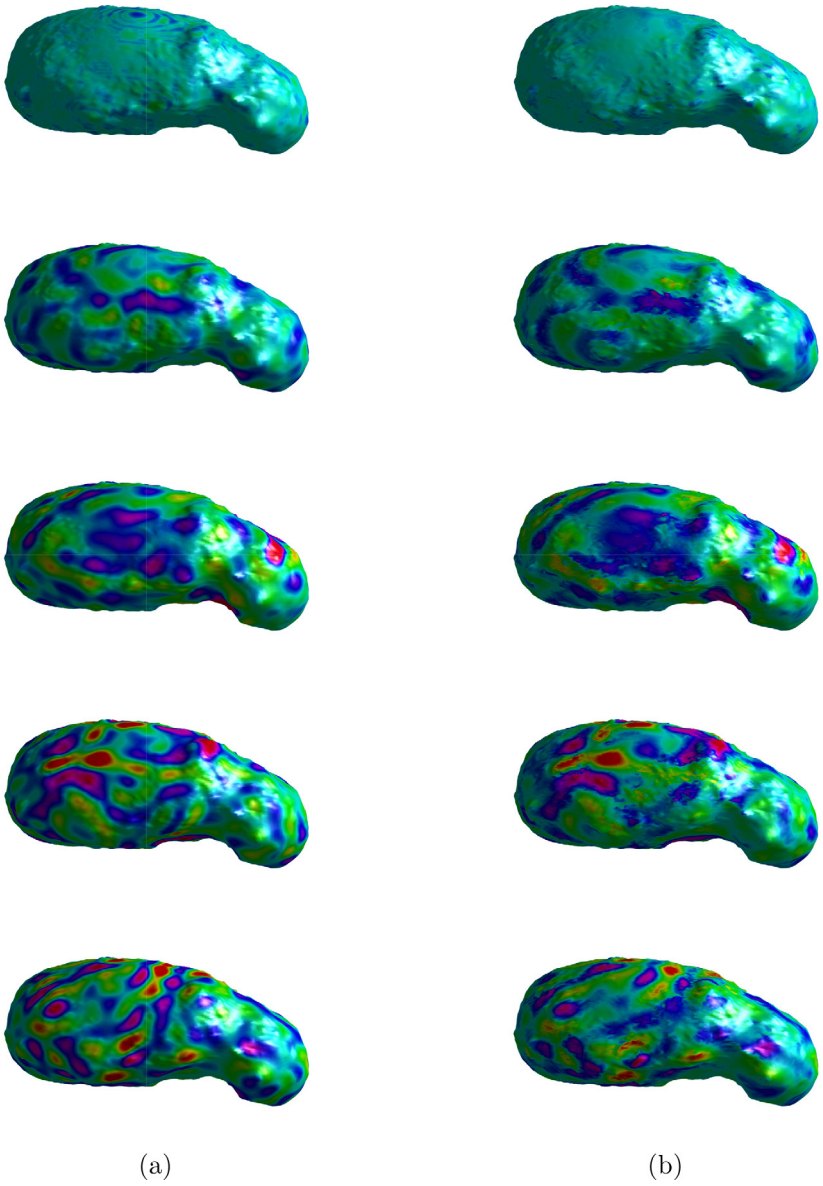


Fig. 10. Radar wavefield snapshots at different times, indicating that the forward simulated wavefields, panels (a), closely resemble the radar wavefields reconstructed from data observed in orbit, panels (b).

to the surface of the comet nucleus, as discussed in the preceding section. Wavefields are sampled densely on the comet nucleus; this sampling is a user-defined parameter, and does not depend on orbital track spacing. We consider wave propagation governed,e.g., by the wave equation Eq. (3). The model we are inverting for is

$$m(\mathbf{x}) = \frac{1}{v^2(\mathbf{x})}, \tag{12}$$

representing slowness squared. This is not the only possible model parameterization, but just a choice that simplifies the solution to the tomographic problem. We can easily transform an inverted model to other parameters, e.g. velocity or dielectric parameters.

The key idea underlying our tomographic approach is that we know a priori and with high precision the exterior shape of the comet nucleus. The standard of 3D shape model reconstruction is nowadays much better than 1 m, therefore shape model errors are not expected to have any significant impact. Then, we can impose the condition that using the datumed data available on the nucleus surface we can image the nucleus surface reflector at the correct position, Fig. 6(b).

One possible definition of the wavefield tomography objective function is

$$J(\mathbf{m}) = \frac{1}{2}\|\mathbf{W_d}\left(\mathbf{d}^{obs} - \mathbf{d}^{pre}(\mathbf{m})\right)\|^2, \tag{13}$$

where the vectors $\mathbf{d}^{obs}$ and $\mathbf{d}^{pre}$ represent the datumed and predicted data on the nucleus surface, respectively, and $\mathbf{W_d}$ is a weighting operator related to the data covariance, characterizing observation uncertainties. The quantity $\mathbf{m}$

represents the model parameters at every location inside the nucleus. The predicted data on the nucleus surface $\mathbf{d}^{pre}$ depends on the current model $\mathbf{m}$. As discussed earlier, the datumed wavefields are dominated by contributions from the surface reflector, which sits at the interface between free space and nucleus materials. Other interior reflectors contribute, as well, but are significantly (one order of magnitude or more) weaker than the boundary reflections.

We can predict the wavefields that would be observed on the comet nucleus using the assumed wave equation. The source function for the exploding reflector model is constructed on the nucleus contour from the local reflectivity $r(\mathbf{s})$ and the radar wavelet $w(t)$:

$$f(\mathbf{s},t) = r(\mathbf{s})\, w(t). \tag{14}$$

Both quantities r and w can be assumed to be known: the wavelet is known from the radar parameters, and the reflectivity is known from direct radar reflections off the nucleus surface. Forward modeling using an assumed interior model predicts the wavefield on the nucleus contour, where they can be compared with the datumed wavefield at every location. If the assumed model is correct, the observed and predicted wavefields are similar to one-another, thus minimizing the objective function from Eq. (13).

We can obtain the optimum model by minimizing the objective function from Eq. (13). This can be accomplished using iterative numeric optimization:

$$\mathbf{m}_{k+1} = \mathbf{m}_k + \alpha_k \mathbf{g}_k, \tag{15}$$

where $\mathbf{g}_k$ is a vector indicating a search direction in which the objective function decreases, and k is the iteration number. This direction depends on the local gradient of the objective function, as well as previous search directions, and can be used to search for an optimal solution using known descent techniques, e.g. the Broyden–Fletcher–Gol dfarb–Shanno (BFGS) method (Fletcher, 1987; Nocedal and Wright, 2000).

An efficient way to evaluate numerically the gradient of the objective function Eq. (13) is the adjoint state method (Tarantola, 1984; Tromp et al., 2005; Plessix, 2006; Virieux and Operto, 2009; Tape et al., 2009). This method is efficient because it bypasses direct computation of Fréchet derivatives. Instead, the adjoint state method allows for gradient calculation just by simulating radar wavefields from the known data and using the current model of physical properties. Specifically, the objective function Eq. (13) leads to an adjoint source, which can be used to construct an adjoint wavefield $a(\mathbf{x},t)$ by solving the wave equation Eq. (3) backward in time. Similarly, we construct a state wavefield $u(\mathbf{x},t)$ by solving the same wave equation forward in time. Correlation between the state and adjoint wavefields leads to the objective function gradient

$$\nabla J(\mathbf{x}) = \sum_{\tau} \delta(\tau)[\ddot{u}(\mathbf{x},t) \bigstar a(\mathbf{x},t)], \tag{16}$$

where the symbol ★ indicates temporal cross-correlation, and τ represents the time lag. The objective function gradient is simply the zero-lag of the cross-correlation between the forward and adjoint wavefields with appropriate time derivatives. In practice, we precondition the objective function gradient in order to insure that the updated models satisfy the Courant–Friedrichs–Lewy conditions (Courant et al., 1967) needed for wavefield simulation stability.

An essential attribute of our tomographic method is that we constrain the physical parameters in the interior of the

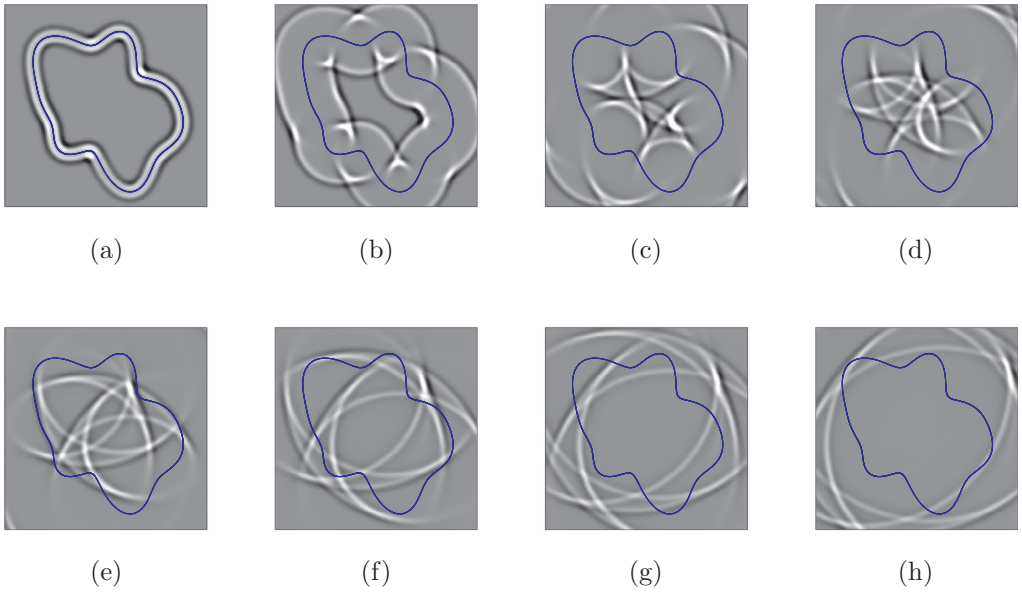


Fig. 11. Schematic representation of wavefields traversing a comet nucleus in multiple directions. Panels (a)–(h) show snapshots of exploding reflector wavefields illuminating the interior of a comet nucleus in many different directions. Each panel shows the wavefield at another (increasing) time. The dark line indicates the contour of the comet nucleus.

nucleus from a closed surface. Therefore, the model parameters are constrained in the interior of the nucleus from all possible directions. Fig. 11 illustrates this idea using wavefields generated using the exploding reflector model for a 2D synthetic shape. Different components of the wavefield originating on its contour intersect throughout the comet nucleus, thus providing constraints of the interior physical properties comparable to the action of a medical tomograph. The more complex the shape of the nucleus, the more diverse the propagation directions in its interior, Fig. 12. Multiple reverberations from the exterior contour of the nucleus further increase interior illumination, albeit at lower amplitude.

Another key idea of our technique is that we are linking through wave propagation information available on opposite sides of the nucleus exterior contour. Specifically, the datumed wavefield observed at a given location on the contour corresponds to exploding reflectors all around the nucleus, but primarily on the opposite side, since the exploding reflectors emit waves in the normal direction relative to the exploding interface. Thus, our technique amounts to a form of transmission tomography, despite the fact that we are using monostatic reflection data. This is only possible because we know a priori the shape of the comet nucleus and we exploit the properties of the exploding reflector model.

Fig. 13 demonstrates this feature. Fig. 13(a)–(h) depict the gradient of the objective function Eq. (13) for different portions of the nucleus contour, showing band-limited sensitivity along different trajectories crossing the nucleus in directions nearly-orthogonal to the contour. Fig. 13(i) shows the total gradient corresponding to the entire nucleus contour, which compares well with the true model perturbation considered in this simplified synthetic demonstration, Fig. 13(j).

The wavefield tomography described here belongs to the class of techniques known as full waveform inversion (FWI). Such techniques are used routinely in terrestrial seismology, both at exploration scale (Berkhout, 1982; Clærbout, 1985), or at global scale (Dahlen and Tromp, 1998; Nolet, 2008). Our modifications to the wavefield tomography problem take advantage of features specific to the comet nucleus problem, i.e. we know the surface contour, and reflection data are available all around the nucleus.

Nevertheless, our technique inherits essential features of FWI, in particular the requirement that the observed and predicted wavefields be close to one-another, i.e. within a fraction of a cycle. This requirement applies to the entire propagation path crossing the comet nucleus. The longer the propagation path, and/or the larger the contrast of physical properties along this path, the higher the likelihood that the predicted and observed wavefield differences are greater than a fraction of a cycle.

One way to mitigate this effect is to lower the frequency band when predicting data with poorly-known models, and to raise the frequency when the model is better known (Bunks et al., 1995; Plessix, 2006; Fichtner et al., 2013). This multiscale technique is highly effective and allows characterization of models with large contrasts from unknown (e.g. constant) initial models.

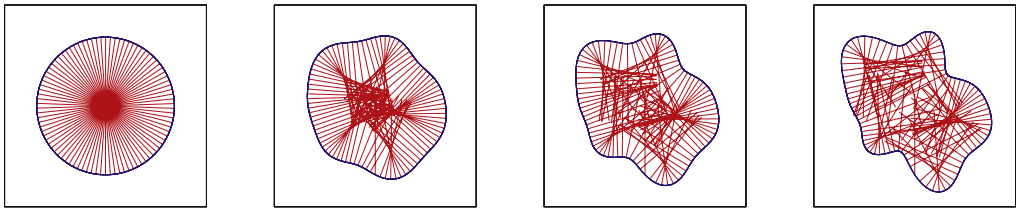
The following example illustrates this multiscale approach for the model depicted in Fig. 7(a). The interior of the model consists of two materials with relative dielectric permittivities ϵ_r of 1.8 and 1.4, corresponding to different types of ice (Stillman et al., 2010). Permittivities can be converted to electromagnetic wave speeds of 0.22 and 0.25 km/μs using

$$\sqrt{\epsilon_r} = \frac{c}{v}, \tag{17}$$

where $c = 0.299$ km/μs represents the speed of light in vacuum. We use two scales for wavefield tomography, corresponding to radar waves with peak frequencies at 5 MHz and 15 MHz. In both cases, we use Ricker wavelets (Ricker, 1944, 1953), in order to avoid truncations of the wavelet frequency spectrum that result in long temporal reverberations.

Fig. 14(a)–(d) illustrate the first scale of the inversion, with wavelet peak amplitude at 5 MHz. The starting model, Fig. 14(c), is constant and chosen to represent a reference material with $\epsilon_r = 1.6$, corresponding to a propagation speed of 0.24 km/μs. The inverted model, Fig. 14(d), depicts some of the essential model features, but at relatively low resolution due to the low frequency used to constrain the model properties.

Finally, Fig. 15(a)–(d) illustrate the second scale of the inversion, with wavelet peak amplitude at 15 MHz. In this case the starting model, Fig. 15(c), is the final model from the preceding scale, Fig. 15(d). The inverted model, Fig. 15



(a) (b) (c) (d)

Fig. 12. Increasingly complex comet shapes lead to more diverse interior illumination directions. A perfectly circular/spherical shape is the worst-case scenario.

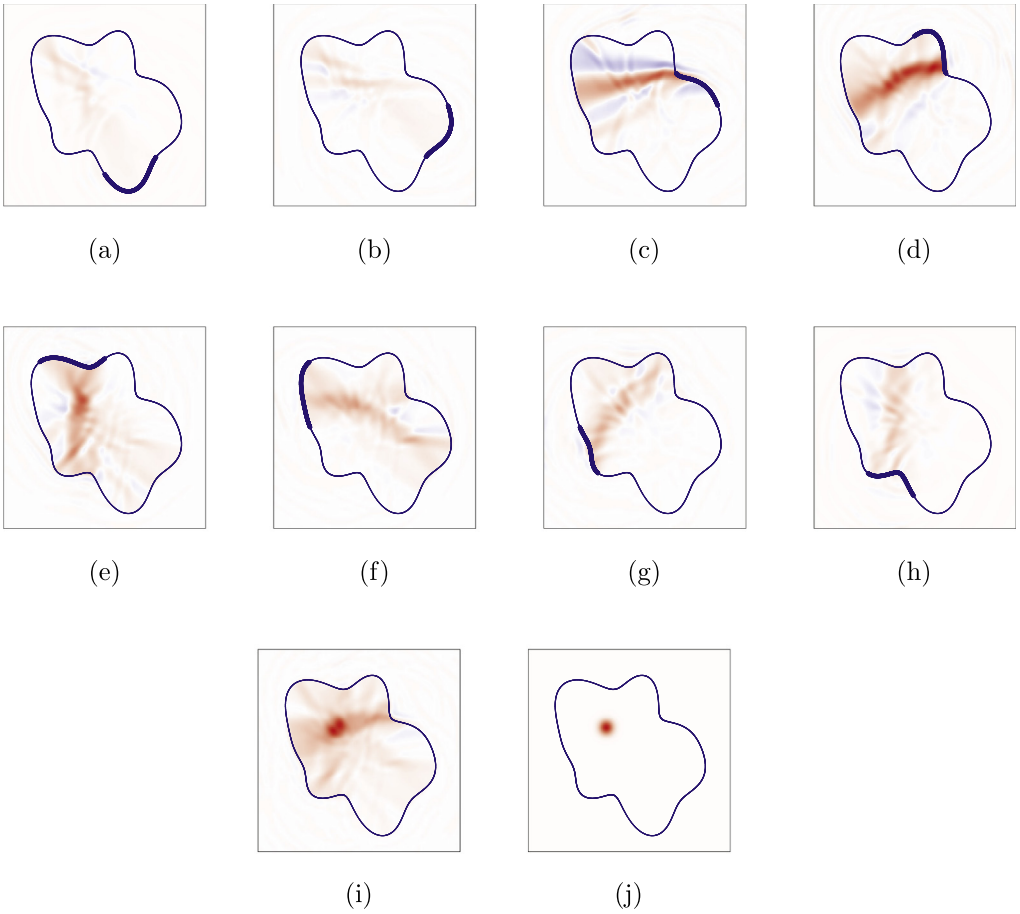


Fig. 13. Illustration of the transmission character for our tomographic technique defined using monostatic radar reflection data. Panels (a)–(h) show the gradient of the tomographic objective function for different portions of the nucleus contour; panel (i) shows the total gradient, which compares well with the assumed model perturbation shown in panel (j). Panels (i) and (j) are on a different color scale than panels (a)-(h).

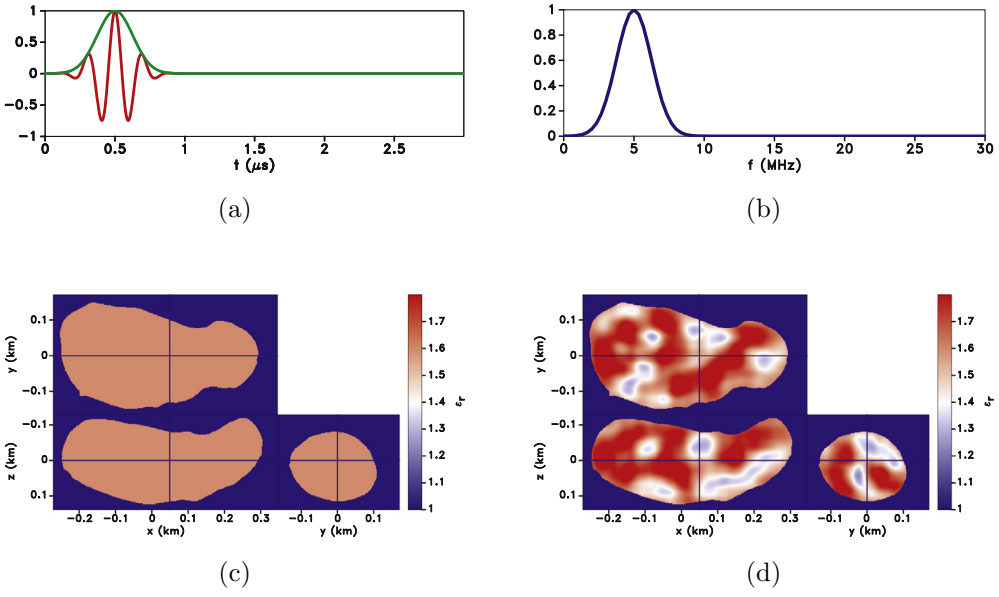


Fig. 14. Wavefield tomography in the frequency band centered at **5 MHz**. (a) Source function and (b) its spectrum; (c) starting model and (d) inverted model. The starting model is constant.

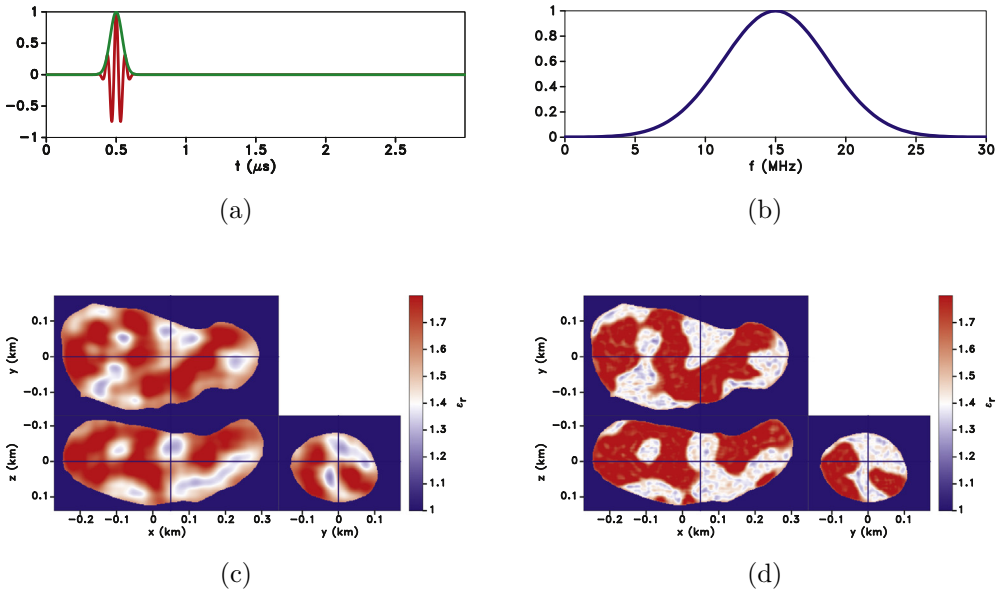


Fig. 15. Wavefield tomography in the frequency band centered at **15 MHz**. (a) Source function and (b) its spectrum; (c) starting model and (d) inverted model. Panel (c) represents the final model obtained at the preceding scale, Fig. 14(d).

(d), captures all model features at nearly the resolution of the original model, Fig. 7(a).

7. Conclusions

High resolution 3D radar imaging can reveal the detailed interior structure of comet nuclei, and thus provide the scientific foundation to answer fundamental questions about the origin and evolution of the Solar system. Such resolution can be accomplished using wavefield tomography based on several key ideas: (1) The comet tomography problem with orbital radar is intrinsically 3D. (2) The orbital data can be efficiently datumed to the nucleus surface, accounting for the antenna radiation pattern and spherical divergence. Data could also be interpolated during datuming to compensate for potentially coarse orbital data sampling. (3) Exploiting the known complex exterior shape of the comet nucleus and the exploding reflector model concept enables transmission tomography based on monostatic radar data. (4) Wavefield tomography at different frequency bands can provide imaging at a resolution comparable with what could be accomplished by bi/multi-static systems. Taken together, these techniques can form the foundation of an effective 3D high-resolution radar space tomograph for detailed interior imaging of comet nuclei.

Acknowledgment

This work was conducted with support from the Center for Wave Phenomena at Colorado School of Mines. The reproducible numeric examples in this paper use the Madagascar open-source software package (Fomel et al., 2013), freely available from www.ahay.org.

References

A'Hearn, M.F., Millis, R.C., Schleicher, D.O., Osip, D.J., Birch, P.V., 1995. The ensemble properties of comets: results from narrowband photometry of 85 comets, 1976–1992. Icarus 118 (2), 223–270.

Aki, K., Richards, P., 2002. Quantitative Seismology, second ed. University Science Books.

Asphaug, E., Oct. 2010. Comet radar explorer. In: AAS/Division for Planetary Sciences Meeting Abstracts. vol. 42, p. 49.32.

Asphaug, E., Barucci, A., Belton, M., Bhaskaran, S., Brownlee, D., Carter, L., Castillo, J., Chelsey, S., Chodas, P., Farnham, T., Gaskell, R., Gim, Y., Heggy, E., Klaasen, K., Kofman, W., Krelavsky, M., Lisse, C., MxFadden, L., Pettinelli, E., Plaut, J., Scheeres, D., Turtle, E., Weissman, P., Wu, R., 2010. Deep Interior Radar Imaging of Comets. In: Lunar and Planetary Science Conference, p. 2670.

Bar-Cohen, Y., 2016. Low Temperature Materials and Mechanisms. CRC Press.

Belton, M.J., Thomas, P., Veverka, J., Schultz, P., A'Hearn, M.F., Feaga, L., Farnham, T., Groussin, O., Li, J.-Y., Lisse, C., McFadden, L., Sunshine, J., Meech, K.J., Delamere, W.A., Kissel, J., 2007. The internal structure of Jupiter family cometary nuclei from Deep Impact observations: the "talps" or "layered pile" model. Icarus 187 (1), 332–344.

Berkhout, A.J., 1982. Imaging of Acoustic Energy by Wave Field Extrapolation. Elsevier.

Bibring, J.-P., Taylor, M.G.G.T., Alexander, C., Auster, U., Biele, J., Finzi, A.E., Goesmann, F., Klingelhoefer, G., Kofman, W., Mottola, S., Seidensticker, K.J., Spohn, T., Wright, I., 2015. Philae's first days on the comet. Science 349 (6247), 493.

Biele, J., Ulamec, S., Maibaum, M., Roll, R., Witte, L., Jurado, E., Muñoz, P., Arnold, W., Auster, H.-U., Casas, C., Faber, C., Fantinati, C., Finke, F., Fischer, H.-H., Geurts, K., Güttler, C., Heinisch, P., Herique, A., Hviid, S., Kargl, G., Knapmeyer, M., Knollenberg, J., Kofman, W., Kömle, N., Kührt, E., Lommatsch, V., Mottola, S., Pardo de Santayana, R., Remetean, E., Scholten, F., Seidensticker, K. J., Sierks, H., Spohn, T., 2015. The landing(s) of Philae and inferences about comet surface mechanical properties 349 (6247).

Blum, J., Gundlach, B., Krause, M., Fulle, M., A, J., Agarwal, J., von Borstel, I., Shi, X., Hu, X., Bentley, M., Capaccioni, F., 2017. Evidence for the formation of comet 67P/Churyumov-Gerasimenko

through gravitational collapse of a bound clump of pebbles. Mon. Not. R. Astron. Soc. 469 (Suppl 2), S755–S773.
Bottke, W.F., Vokrouhlick, D., Nesvorn, D., 2007. An asteroid breakup 160Myr ago as the probable source of the K/T impactor. Nature 449, 48–53.
Bunks, C., Saleck, F.M., Zaleski, S., Chavent, G., 1995. Multiscale seismic waveform inversion. Geophysics 60 (05), 1457–1473.
Ciarletti, V., Herique, A., Lasue, J., Levasseur-Regourd, A.-C., Plettemeier, D., Florentin, L., Christophe, G., Pierre, P., Kofman, W., 2017. Consert constrains the internal structure of 67P at a few-metre size scale. Mon. Not. R. Astron. Soc., stx3132
Clærbout, J.F., 1976. Fundamentals of Geophysical Data Processing. Blackwell Scientific Publications.
Clærbout, J.F., 1985. Imaging the Earth's Interior. Blackwell Scientific Publications.
Courant, R., Friedrichs, K., Lewy, H., 1967. On the partial difference equations of mathematical physics. IBM J. Res. Dev. 11 (2), 215–234.
Dahlen, F.A., Tromp, J., 1998. Theoretical Global Seismology. Princeton University Press.
El-Maarry, M.R., Thomas, N., Giacomini, L., Massironi, M., Pajola, M., Marschall, R., Gracia-Bern, A., Sierks, H., Barbieri, C., Lamy, P.L., Rodrigo, R., Rickman, H., Koschny, D., Keller, H.U., Agarwal, J., A'Hearn, M.F., Auger, A.-T., Barucci, M.A., Bertaux, J.-L., Bertini, I., Besse, S., Bodewits, D., Cremonese, G., Da Deppo, V., Davidsson, B., De Cecco, M., Debei, S., Güttler, C., Fornasier, S., Fulle, M., Groussin, O., Gutierrez, P.J., Hviid, S.F., Ip, W.-H., Jorda, L., Knollenberg, J., Kovacs, G., Kramm, J.-R., Kührt, E., Küppers, M., La Forgia, F., Lara, L.M., Lazzarin, M., Lopez Moreno, J.J., Marchi, S., Marzari, F., Michalik, H., Naletto, G., Oklay, N., Pommerol, A., Preusker, F., Scholten, F., Tubiana, C., Vincent, J.-B., 2015. Regional surface morphology of comet 67P/Churyumov-Gerasimenko from Rosetta/OSIRIS images. Astron. Astrophys. 583, A26.
Fichtner, A., Trampert, J., Cupillard, P., Saygin, E., Taymaz, T., Capdeville, Y., Villaseor, A., 2013. Multiscale full waveform inversion. Geophys. J. Int. 194 (1), 534–556.
Fletcher, R., 1987. Practical Methods of Optimization. Wiley.
Fomel, S., Sava, P.C., Vlad, I., Liu, Y., Bashkardin, V., 2013. Madagascar: open-source software project for multidimensional data analysis and reproducible computational experiments. J. Open Res. Software 1 (1), e8.
Foss, F.J., Putzig, N.E., Campbell, B.A., Phillips, R.J., 2017. 3D imaging of Mars' polar ice caps using orbital radar data. Lead. Edge 36 (1), 43–57.
Gauthier, O., Virieux, J., Tarantola, A., 1986. Two-dimensional nonlinear inversion of seismic waveforms – numerical results. Geophysics 51 (07), 1387–1403.
Glassmeier, K.-H., Boehnhardt, H., Koschny, D., Kührt, E., Richter, I., 2007. The Rosetta mission: flying towards the origin of the solar system. Space Sci. Rev. 128 (1), 1–21.
Grimm, R., Stillman, D., Sava, P.C., Ittharat, D., 2015. Radio reflection imaging of asteroid and comet interiors II: Results and Recommendations. Adv. Space Res. 55, 2166–2176.
Heggy, E., Palmer, E.M., Kofman, W., Clifford, S.M., Righter, K., Hrique, A., 2012. Radar properties of comets: parametric dielectric modeling of comet 67p/churyumov–gerasimenko. Icarus 221 (2), 925–939.
Herique, A., Kofman, W., Beck, P., Bonal, L., Buttarazzi, I., Heggy, E., Lasue, J., Levasseur-Regourd, A.C., Quirico, E., Zine, S., 2016. Cosmochemical implications of CONSERT permittivity characterization of 67P/CG. Mon. Not. R. Astron. Soc. 462 (Suppl 1), S516–S532.
Jol, H., 2008. Ground Penetrating Radar Theory and Applications. Elsevier.
Jutzi, M., Asphaug, E., 2015. The shape and structure of cometary nuclei as a result of low-velocity accretion. Science 348 (6241), 1355–1358.
Kofman, W., Herique, A., Barbin, Y., Barriot, J.-P., Ciarletti, V., Clifford, S., Edenhofer, P., Elachi, C., Eyraud, C., Goutail, J.-P., Heggy, E., Jorda, L., Lasue, J., Levasseur-Regourd, A.-C., Nielsen, E., Pasquero, P., Preusker, F., Puget, P., Plettemeier, D., Rogez, Y., Sierks, H., Statz, C., Svedhem, H., Williams, I., Zine, S., Van Zyl, J., 2015. Properties of the 67P/Churyumov-Gerasimenko interior revealed by CONSERT radar. Science 349 (6247).
Kofman, W., Herique, A., Goutail, J.-P., Hagfors, T., Williams, I.P., Nielsen, E., Barriot, J.-P., Barbin, Y., Elachi, C., Edenhofer, P., Levasseur-Regourd, A.-C., Plettemeier, D., Picardi, G., Seu, R., Svedhem, V., 2007. The Comet Nucleus Sounding Experiment by Radiowave Transmission (CONSERT): A short description of the instrument and of the commissioning stages. Space Sci. Rev. 128, 413–432.
Kofman, W., Safaeinili, A., 2004. Peering inside near-Earth objects with radio tomography. In: Mitigiation of Hazardous Comets and Asteroids. Cambridge University Press.
Levison, H.F., Duncan, M.J., 1997. From the Kuiper Belt to Jupiter-Family Comets: the spatial distribution of ecliptic comets. Icarus 127 (1), 13–32.
Massironi, M., Simioni, E., Marzari, F., Cremonese, G., Giacomini, L., Pajola, M., Jorda, L., Naletto, G., Lowry, S., El-Maarry, M.R., Preusker, F., Scholten, F., Sierks, H., Barbieri, C., Lamy, P., Rodrigo, R., Koschny, D., Keller, H.R.H.U., A'Hearn, M.F., Agarwal, J., Auger, A.-T., Barucci, M.A., Bertaux, J.-L., Bertini, I., Besse, S., Bodewits, D., Capanna, C., Deppo, V.D., Davidsson, B., Debei, S., Cecco, M.D., Ferri, F., Fornasier, S., Fulle, M., Gaskell, R., Groussin, O., Gutiérrez, P.J., Güttler, C., Hviid, S.F., Ip, W.-H., Knollenberg, J., Kovacs, G., Kramm, R., Kührt, E., Küppers, M., Forgia, F.L., Lara, L.M., Lazzarin, M., Lin, Z.-Y., Moreno, J.J.L., Magrin, S., Michalik, H., Mottola, S., Oklay, N., Pommerol, A., Thomas, N., Tubiana, C., Vincent, J.-B., 2015. Two independent and primitive envelopes of the bilobate nucleus of comet 67P. Nature 526, 402–405.
Miller, R.D., Bradford, J.H., (Eds.), K.H., 2010. Advances in near-surface seismology and ground-penetrating radar. Soc. Explor. Geophys.
Morbidelli, A., Rickman, H., 2015. Comets as collisional fragments of a primordial planetesimal disk. Astron. Astrophys. 583, A43.
Nocedal, J., Wright, S.J., 2000. Numerical Optimization. Springer.
Nolet, G., 2008. A Breviary of Seismic Tomography: Imaging the Interior of the Earth and Sun. Cambridge University Press.
Operto, S., Ravaut, C., Improta, L., Virieux, J., Herrero, A., DellAversana, P., 2004. Quantitative imaging of complex structures from dense wide-aperture seismic data by multiscale traveltime and waveform inversions: a case study. Geophys. Prosp. 52 (6), 625–651.
Phillips, R.J., Davis, B.J., Tanaka, K.L., Byrne, S., Mellon, M.T., Putzig, N.E., Haberle, R.M., Kahre, M.A., Campbell, B.A., Carter, L.M., Smith, I.B., Holt, J.W., Smrekar, S.E., Nunes, D.C., Plaut, J.J., Egan, A.F., Titus, T.N., Seu, R., 2011. Massive CO_2 ice deposits sequestered in the South Polar Layered Deposits of Mars. Science 332 (6031), 838–841.
Plaut, J.J., Safaeinili, A., Holt, J.W., Phillips, R.J., Head, J.W., Seu, R., Putzig, N.E., Frigeri, A., 2009. Radar evidence for ice in lobate debris aprons in the mid-northern latitudes of Mars. Geophys. Res. Lett. 36 (2), L02203.
Plessix, R.-E., 2006. A review of the adjoint state method for computing the gradient of a functional with geophysical applications. Geophys. J. Int. 167, 495–503.
Prati, C., Rocca, F., Guarnieri, A.M., Damonti, E., 1990. Seismic migration for SAR focusing: interferometrical applications. IEEE Trans. Geosci. Remote Sens. 28 (4).
Pratt, R.G., 1999. Seismic waveform inversion in the frequency domain, Part 1: Theory and verification in a physical scale model. Geophysics 64 (3), 888–901.
Pratt, R.G., Worthington, M.H., 1990. Inverse theory applied to multisource cross-hole tomography. Part 1: Acoustic wave-equation method. Geophys. Prosp. 38 (03), 287–310.
Preusker, F., Scholten, F., Matz, K.-D., Roatsch, T., Willner, K., Hviid, S.F., Knollenberg, J., Jorda, L., Gutiérrez, P.J., Kührt, E., Mottola, S., A'Hearn, M.F., Thomas, N., Sierks, H., Barbieri, C., Lamy, P., Rodrigo, R., Koschny, D., Rickman, H., Keller, H.U., Agarwal, J.,

Barucci, Bertaux, J.-L., Bertini, I., Cremonese, G., Da Deppo, V., Davidsson, B., Debei, S., De Cecco, M., Fornasier, S., Fulle, M., Groussin, O., Güttler, C., Ip, W.-H., Kramm, J.R., Küppers, M., Lara, L.M., Lazzarin, M., Lopez Moreno, J.J., Marzari, F., Michalik, H., Naletto, G., Oklay, N., Tubiana, C., Vincent, J.-B., 2013. Shape model, reference system definition, and cartographic mapping standards for comet 67P/Churyumov-Gerasimenko – Stereo-photogrammetric analysis of Rosetta/OSIRIS image data. Astron. Astrophys. 583, A33.

Reynolds, J.M., 2011. An Introduction to Applied and Environmental Geophysics, second ed. Wiley.

Ricker, N., 1944. Wavelet functions and their polynomials. Geophysics 9 (3), 314–323.

Ricker, N., 1953. Wavelet contraction, wavelet expansion, and the control of seismic resolution. Geophysics 18 (4), 769–792.

Safaeinili, A., Gulkis, S., Hofstadter, M., Jordsn, R., 2002. Probing the interior of asteroids and comets using radio reflection tomography. Meteor. Planet. Sci. 37, 1953–1963.

Samarasinha, N.H., Belton, M.J., 1995. Long-term evolution of rotational states and nongravitational effects for Halley-like cometary nuclei. Icarus 116 (2), 340–358.

Sava, P.C., Biondi, B., 2004. Wave-equation migration velocity analysis – I: theory. Geophys. Prospect. 52, 593–606.

Sava, P.C., Ittharat, D., Grimm, R., Stillman, D., 2015. Radio reflection imaging of asteroid and comet interiors I: acquisition and imaging theory. Adv. Space Res. 55, 2149–2165.

Scheeres, D., Marzari, F., Tomasella, L., Vanzani, V., 1998. ROSETTA mission: satellite orbits around a cometary nucleus. Planet. Space Sci. 46 (6), 649–671.

Sierks, H., Barbieri, C., Lamy, P.L., Rodrigo, R., Koschny, D., Rickman, H., Keller, H.U., Agarwal, J., A'Hearn, M.F., Angrilli, F., Auger, A.-T., Barucci, M.A., Bertaux, J.-L., Bertini, I., Besse, S., Bodewits, D., Capanna, C., Cremonese, G., Da Deppo, V., Davidsson, B., Debei, S., De Cecco, M., Ferri, F., Fornasier, S., Fulle, M., Gaskell, R., Giacomini, L., Groussin, O., Gutierrez-Marques, P., Gutiérrez, P.J., Güttler, C., Hoekzema, N., Hviid, S.F., Ip, W.-H., Jorda, L., Knollenberg, J., Kovacs, G., Kramm, J.R., Kührt, E., Küppers, M., La Forgia, F., Lara, L.M., Lazzarin, M., Leyrat, C., Lopez Moreno, J. J., Magrin, S., Marchi, S., Marzari, F., Massironi, M., Michalik, H., Moissl, R., Mottola, S., Naletto, G., Oklay, N., Pajola, M., Pertile, M., Preusker, F., Sabau, L., Scholten, F., Snodgrass, C., Thomas, N., Tubiana, C., Vincent, J.-B., Wenzel, K.-P., Zaccariotto, M., Pätzold, M., 2015. On the nucleus structure and activity of comet 67PSierk-saaa1044/Churyumov-Gerasimenko. Science 347 (6220).

Sirgue, L., Pratt, R., 2004. Efficient waveform inversion and imaging: a strategy for selecting temporal frequencies. Geophysics 69 (1), 231–248.

Smith, D.E., Zuber, M.T., Frey, H.V., Garvin, J.B., Head, J.W., Muhleman, D.O., Pettengill, G.H., Phillips, R.J., Solomon, S.C., Zwally, H.J., Banerdt, W.B., Duxbury, T.C., Golombek, M.P., Lemoine, F.G., Neumann, G.A., Rowlands, D.D., Aharonson, O., Ford, P.G., Ivanov, A.B., Johnson, C.L., McGovern, P.J., Abshire, J. B., Afzal, R.S., Sun, X., 2001. Mars Orbiter Laser Altimeter: Experiment summary after the first year of global mapping of Mars. J. Geophys. Res.: Planets 106 (E10), 23689–23722.

Smith, D.E., Zuber, M.T., Neumann, G.A., Lemoine, F.G., Mazarico, E., Torrence, M.H., McGarry, J.F., Rowlands, D.D., Head, J.W., Duxbury, T.H., Aharonson, O., Lucey, P.G., Robinson, M.S., Barnouin, O.S., Cavanaugh, J.F., Sun, X., Liiva, P., Mao, D.-d., Smith, J.C., Bartels, A.E., 2010. Initial observations from the Lunar Orbiter Laser Altimeter (LOLA). Geophys. Res. Lett. 37 (18), l18204.

Stillman, D.E., Grimm, R.E., Dec, S.F., 2010. Low-frequency electrical properties of ice-silicate mixtures. J. Phys. Chem. B 114 (18), 6065–6073.

Tape, C., Liu, Q., Maggi, A., Tromp, J., 2009. Adjoint tomography of the Southern California crust. Science 325 (5943), 988–992.

Tarantola, A., 1984. Inversion of seismic reflection data in the acoustic approximation. Geophysics 49 (08), 1259–1266.

Tarantola, A., 1987. Inverse Problem Theory: Methods for Data Fitting and Model Parameter estimation. Elsevier.

Tromp, J., Tape, C., Liu, Q., 2005. Seismic tomography, adjoint methods, time reversal and banana-doughnut kernels. Geophys. J. Int. 160 (1), 195–216.

Virieux, J., Operto, S., 2009. An overview of full-waveform inversion in exploration geophysics. Geophysics 74 (6), WCC1–WCC26.

Weidenschilling, S., 1997. The origin of comets in the solar nebula: a unified model. Icarus 127 (2), 290–306.

Weissman, P.R., 1986. Are cometary nuclei primordial rubble piles? Nature 320, 242–244.

Woodward, M.J., 1992. Wave-equation tomography. Geophysics 57 (01), 15–26.

Zuber, M.T., Smith, D.E., Watkins, M.M., Asmar, S.W., Konopliv, A.S., Lemoine, F.G., Melosh, H.J., Neumann, G.A., Phillips, R.J., Solomon, S.C., Wieczorek, M.A., Williams, J.G., Goossens, S.J., Kruizinga, G., Mazarico, E., Park, R.S., Yuan, D.-N., 2013. Gravity field of the Moon from the Gravity Recovery and Interior Laboratory (GRAIL) mission. Science 339 (6120), 668–671.